KSCE Journal of Civil Engineering (2023) 27(9):3848-3860
DOI 10.1007/s12205-023-1273-8

pISSN 1226-7988, eISSN 1976-3808
www.springer.com/12205

Railroad Engineering

Performance Evaluation of a Combined Transition System in Slab-Ballasted Railway Track Using a Vehicle-Track-Substructure Interaction Model

Hamidreza Heydari-Noghabi[a], **José Nuno Varandas**[b], **Jabbar Ali Zakeri**[a], **and Morteza Esmaeili**[a]

[a]*Iran University of Science and Technology, Tehran 16846-13114, Narmak, Iran*
[b]*CERIS, Faculdade de Ciências e Tecnologia, Universidade NOVA de Lisboa, 2829-516, Caparica, Portugal*

ARTICLE HISTORY

Received 31 July 2022
Revised 9 November 2022
Accepted 9 December 2022
Published Online 9 August 2023

KEYWORDS

Vehicle-track-substructure interaction
Railway transition zone
Slab-ballasted track
Combined transition system
FE method

ABSTRACT

Abrupt stiffness variations along the railway track may increase the geometrical and mechanical defects of railway lines. The conjunction points of a railway track with concrete and ballast pavements, which are called slab-ballasted track transitions, are one of the main areas where vertical track stiffness changes sharply. Therefore, the potential benefits of a combined transition system along the slab-ballasted transition, made of an approach slab and additional rails, are studied in this paper. For this purpose, a vehicle-track-substructure interaction model, which included three main segments of the railway track (slab track, transition zone, and ballasted track) was programmed based on the finite element method. A test line with the mentioned combined transition system was built to measure the railway track responses through field study. Then, the three-dimensional (3D) numerical model was validated using the results obtained from the experimental tests. Afterwards, a number of parametric studies were performed to analyze the dynamic responses of the combined transition zone. The results indicated that this type of transition system promotes a smoother stiffness transition between the slab track segment and the ballasted track segment by making the transition in three gradual steps. The track displacements in the analyzed case-study gradually increased by about 22%, 28%, and 34% along the combined transition zone in the junction points of the slab and ballasted tracks.

1. Introduction

Studies on railway infrastructures continue to focus on railway transition zones due to the considerable number of different cases they cover, their complex and sometimes poorly understood behavior, and the subpar performance that many transition zones still exhibit. As a result of the rising demand and the development of high-speed lines supported on slab tracks, especially in China, the number of studies dedicated to slab-ballasted track transitions have increased because they are essential for better understanding the behavior of these locations and improving their design.

In general, the problems at railway track transitions are due to differential settlements that develop between the two segments connected by the track transition, which directly lead to dynamic forces acting on the track, poor track geometrical quality, speed restrictions, and increased maintenance efforts (Wang et al., 2015; Varandas et al., 2020). Wang et al. (2017) studied the settlement in different railway transition zones with various conditions through experimental analysis. Wang and Markine (2018a; 2018b) modelled the railway transition zones to predict the short-term and long-term behaviour of track settlement.

Furthermore, if the stiffness transition at these locations changes abruptly and the trains' speeds are very high, unwanted dynamic amplification may occur, which will further amplify the track degradation at these locations, in addition to reducing the lifetime of superstructure components (Sasaoka and Davies, 2005; Lei and Zhang, 2010; Paixão et al., 2013; Haoyu, 2018). This aspect justifies the high number of railway transition studies focused on the stiffness variation.

Reviewing the literature shows that use different methods to solve the mentioned problems in railway transition zone sun as reinforcement subgrade layers (Sañudo et al., 2016; Fei et al., 2019), backfill construction (Paixão et al., 2013), changing the sleeper distances (Shahraki et al., 2015), use of under sleeper pad (Paixão et al., 2015; Heydari et al., 2022), installing of additional rails (Esmaeili et al., 2020), approach slab (Coelho and Hicks,

CORRESPONDENCE Hamidreza Heydari-Noghabi h_heydari@iust.ac.ir Iran University of Science and Technology, Tehran 16846-13114, Narmak, Iran

ⓒ 2022 Korean Society of Civil Engineers

2015) and etc. The most of investigation on railway transition zone performed in ballasted railway track especially at the adjacent of bridges or culverts. One of the transition areas is the slab-ballasted track that its dynamic behavior is lesser investigated in literature and previous studies. So in some technical aspects, there are lacks of knowledge about the performance of slab-ballasted transition systems. Initial numerical studies on the slab-ballasted track transition were performed by Zakeri and Ghorbani (2011), Costa D'Aguiar et al. (2015), and Arlaud et al. (2016) by using a one-dimensional (1D) Winkler-type model, a two-dimensional (2D) plane strain model, and a 3D finite elements (FE) model (Dynavoie), respectively. In these studies, the transient dynamic response at slab-ballasted track transitions was analyzed by assuming the linear-elastic response of the vehicle-track system at these locations and focused on the track stiffness variation. In addition, the study conducted by Aggestam and Nielsen (2019), which focused on the stiffness variation, optimized a slab-ballasted track transition by using a 1D Winkler-type model and genetic algorithms, and in the study by Ngamkhanong et al. (2020), the use of different baseplate fastening systems on the slab track was studied within these types of railway transitions. Shahraki et al. (2015) analyzed the potential benefit of considering sleepers with varying lengths and additional rails at a slab-ballasted track transition, but disregarded the train-track interaction, whereas Xin et al. (2020) considered a Winkler-type model of vehicle-track interaction to numerically analyze the application of rubber mats in order to gradually change the track stiffness in transitions between different types of slab tracks. Walker and Indraratna (2018) attempted to study the railway transition zones by passing several moving loads on a viscoelastic foundation, which was considered as a beam resting on a Winkler spring with dashpot. Esmaeili et al. (2020) investigated a stiffened transition zone along a railway culvert with a 2D model in which the ballasted track and its components were modeled as a series of mass–spring–damper systems. In the study by Heydari et al. (2017), a 3D FEM vehicle-track interaction model of transient dynamic simulation was validated using field measurements performed at a slab-ballasted track transition and was employed to investigate the consideration of additional rails aiming at minimizing the stiffness transition at these locations. Real et al. (2016) assessed the static and dynamic behavior of transitions between different railway track typologies using a 3D FEM.

Most of the abovementioned numerical approaches that referred to study slab-ballasted track transitions assume full linear-elastic behavior of the vehicle-track system. Important non-linearities taking place in railway transitions are the loss of contact between the sleeper and the ballast at the junction segment, the eventual micro-slip with friction of the concrete slab relative to the ballast at the end of the slab, and the supporting granular layer at the bottom of the slab. Another critical limitation in many studies is the consideration of 1D or 2D approaches to analyze a problem that is 3D in nature and that may involve wave propagation phenomena caused by the impact loading at the junction segment. In this work, a 3D model properly addressing these non-linearities is

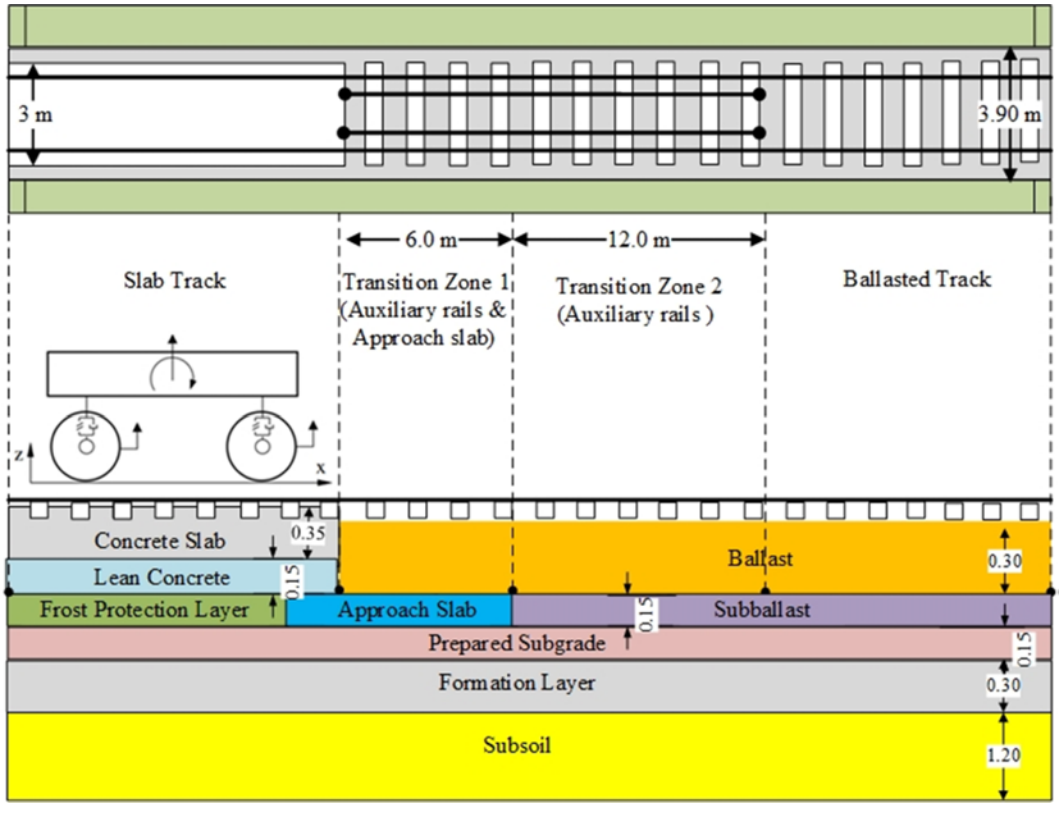

Fig. 1. Schematic Plan and Longitudinal View of the Combined Transition Zone Model

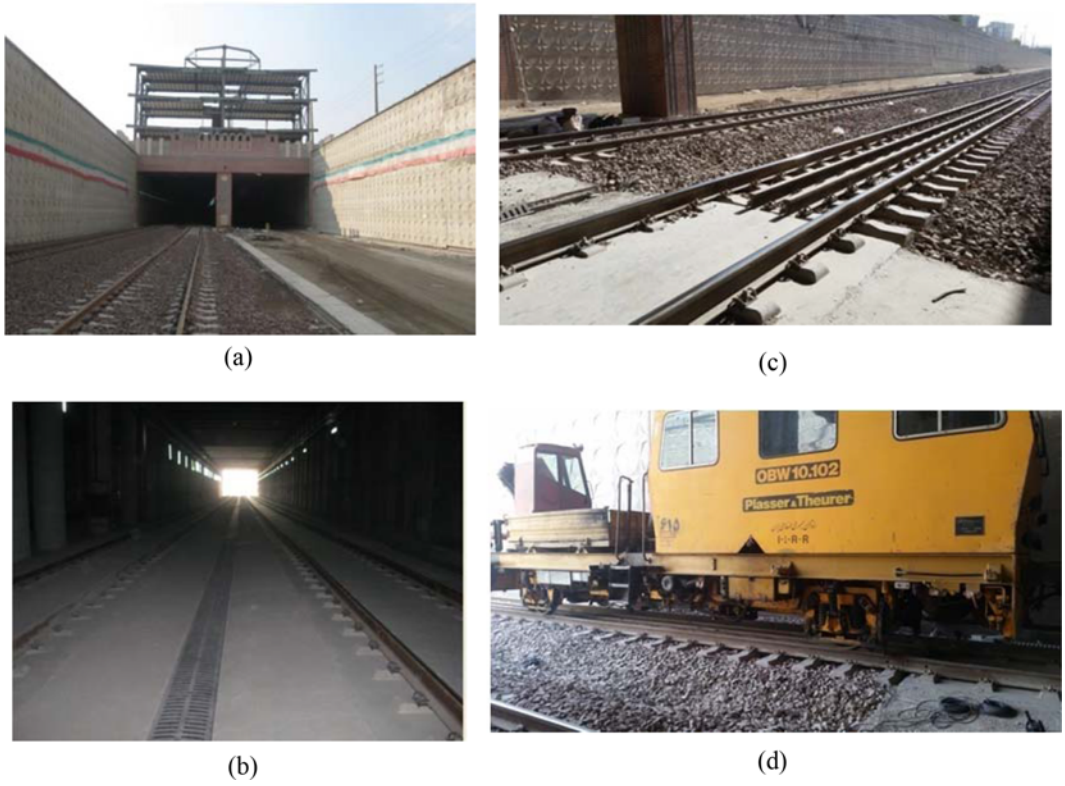

Fig. 2. Test Track: (a) Ballasted Track, (b) Slab Track, (c) Combined Transition Zone, (d) Track Vehicle

used, and an innovative study of using a combined solution to tackle the stiffness transition change is presented. The combined solution consists of adopting auxiliary rails together with an approach slab placed under the ballasted segment of the transition. Then, after the validation of the numerical model, the dynamic effects and the technical performance of this solution of the transition zone are evaluated by several sensitivity analyses, and the summarized results are presented in the end.

2. Methodology of Combined Transition Zone Study

The track transition studied here corresponds to a slab-ballasted track transition formed by auxiliary rails and an approach slab. The schematic plan and longitudinal view of the combined transition zone solution studied in this paper are depicted in Fig. 1. The railway track can be divided into three main segments here: the slab track segment, the transition zone segment, and the ballasted track segment. The transition zone segment can be further separated into two sections: The part of the transition zone next to the slab track segment is made with auxiliary rails and an approach slab, while the part next to the ballasted track segment is made with auxiliary rails only. The auxiliary rails are placed between the main rails.

The slab track section is formed by the rails, a reinforced-steel concrete slab, a lean concrete layer, a frost protection layer (FPL), and the remaining substructure layers. The ballasted track section is formed by the rails, the sleepers, a ballast layer, and the substructure layers. The main layers of the substructure are the prepared subgrade/sub-ballast, a formation layer, and the subsoil.

Table 1. Characteristics of the Track Components in the Numerical Model (Heydari-Noghabi et al., 2017)

Item	Elastic modulus (MPa)	Density (kg/m^3)	v	Thickness (m)
Rail	210,000	7850	0.3	0.152
Slab	30,000	2500	0.2	0.35
Lean concrete	10,000	2200	0.1	0.15
Frost protection layer	110	1900	0.2	0.15
Sleeper	50,000	2500	0.2	0.20
Ballast layer	130	1800	0.2	0.30
Sub-ballast	110	1900	0.2	0.15
Prepared subgrade	100	1900	0.2	0.15
Formation layer	80	1700	0.2	0.30
Subsoil	60	1600	0.2	1.20

A track transition with the mentioned characteristics is located at the entrance of an underground tunnel at the vicinity of Tehran Railway Station. Fig. 2 displays images of this transition, where it can be seen that at the entrance of the tunnel, the superstructure of the railway track changes from ballasted to slab track, with the auxiliary rails clearly visible in Fig. 2(c).

Table 1 lists the characteristics assumed for the track components, including their thickness/height. The rail seat spacing, sleeper length, and concrete slab width were, respectively, 600, 2,600, and 3,000 mm. The railpad stiffness was considered constant and

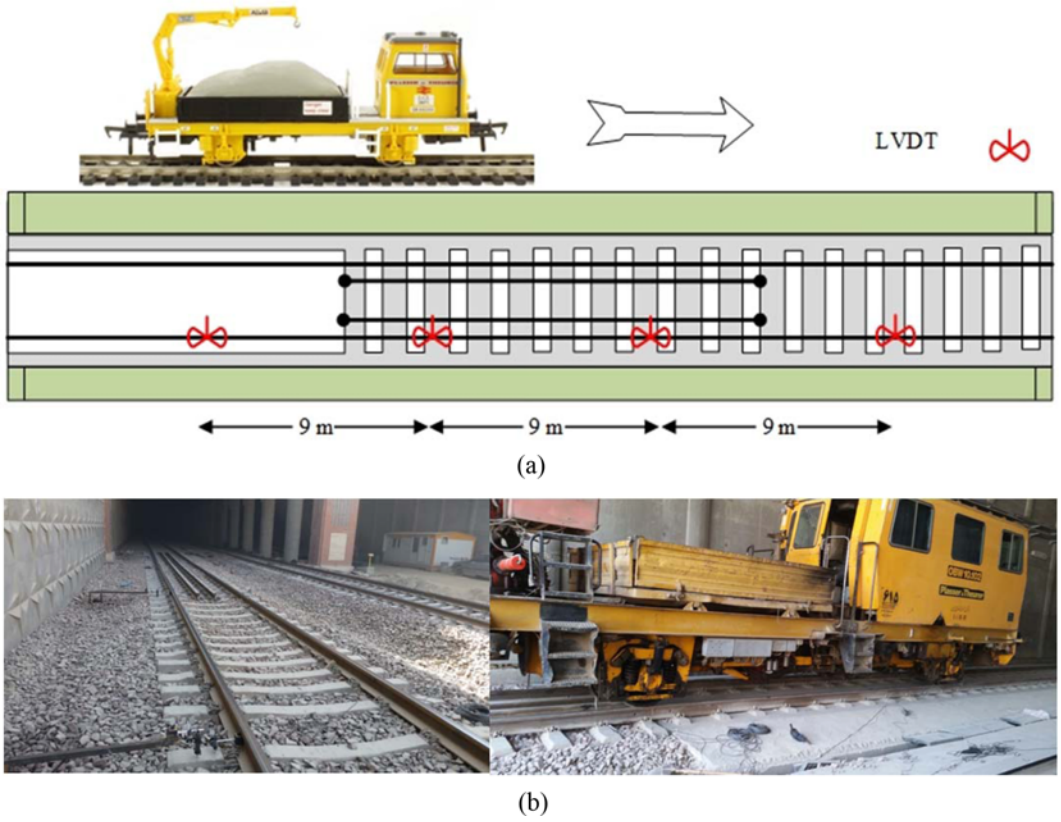

Fig. 3. Experimental Test Along the Combined Transition Zone: (a) Test Plan, (b) Measurement Campaign

equal to 110 kN/mm (both in the slab track and in the ballasted track segment).

This transition was instrumented with displacement transducers (linear variable differential transformers, LVDTs) at four sections as shown in Fig. 3(a). As can be observed in this figure, one LVDT was installed in the slab section, two LVDTs were installed in the middle of the two transition parts, and a fourth LVDT was placed in the ballasted track segment. This arrangement allowed the screening of the track displacements variation when a test vehicle passed by at a low speed. The LVDTs used in this study were the TML type. The measuring was performed by connecting the LVDTs to a laptop and data logger during the experimental tests. The sampling frequency of the acquisition rate was set at the frequency of 2,000 Hz.

Figure 3(b) shows the experimental tests performed when a permanent way motor vehicle was passing through the combined transition zone. The model of this maintenance machine was OBW 10. The OBW 10 has a loading platform and a special crane usually used for track maintenance works. The field measurements and data gatherings were carried out by the passage of this track vehicle at different speeds. The results of the measurement campaign are presented later in the paper, in the validation section.

3. 3D Numerical Model for Vehicle-Track-Substructure Dynamic Analysis

A numerical model of the slab-ballasted track transition case studied here was built with *Pegasus 3D FEM* program developed in the MATLAB (2010) environment. This program was previously presented in several studies, e.g., those by Varandas (2013) and Varandas et al. (2017), but in this work, the *Pegasus 3D FEM* program was extended from previous versions in order to include the concrete slab and the approach slab that forms the transition zone. This section gives a brief description of the model, focusing on the aspects related to the modeling of the slab, whereas additional information can be found in previous references.

3.1 General Description of the Model

Figure 4 shows a schematic view of the numerical model that was used in this study. The numerical model consists of three main subsystems: the vehicle system, the track superstructure system, and the substructure system. The track superstructure and the substructure system are spatially discretized based on the FE method (Hughes, 2003; Bhatti, 2005). The three systems interact with each other through the interaction contacts, as described in the following.

The vehicle model is presented in Fig. 5. The model represents the vehicle that was used during the measurement campaign, which is a railcar with two wheelsets, as shown in Fig. 3. The vehicle model is an assemblage of rigid bodies with seven degrees of freedom, consisting of three translations and four rotations. The mass matrix of the vehicle is derived as a diagonal matrix of order 7:

$$[M_V] = diagonal[M_{w1}\ I_{w1x}\ M_{w2}\ I_{w2x}\ M_b\ I_{bx}\ I_{by}]\,, \qquad (1)$$

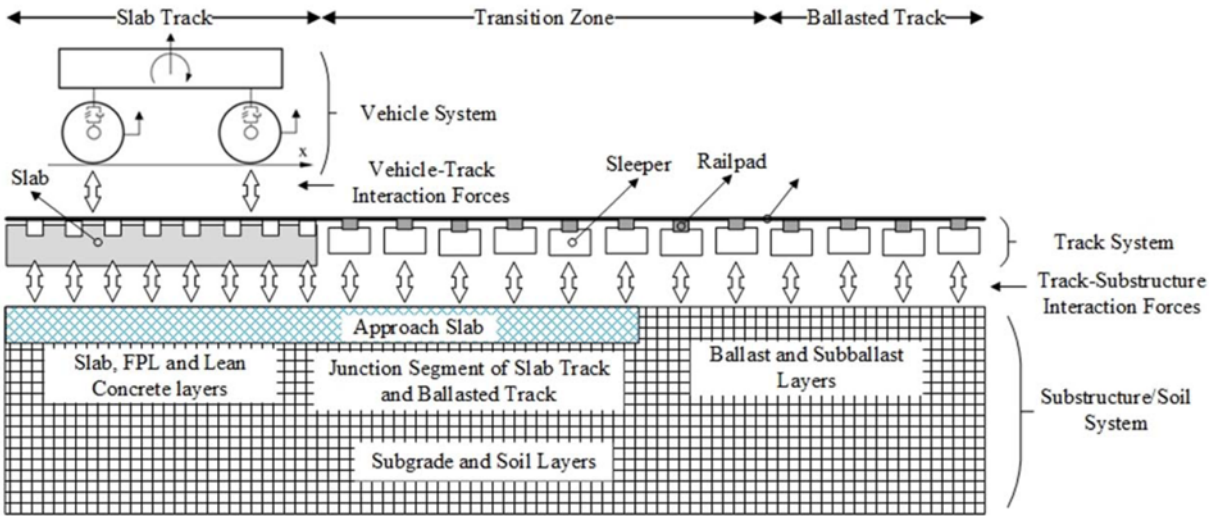

Fig. 4. Schematic View of the Vehicle-Track-Substructure Model

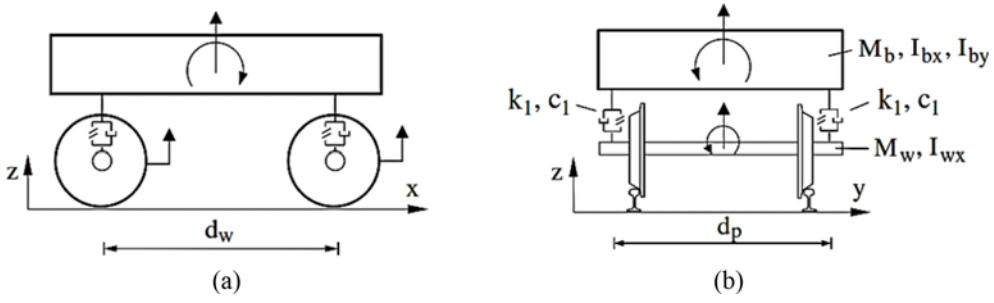

Fig. 5. Vehicle Model Used in Numerical Analysis: (a) Longitudinal View, (b) Front View

where x and y denote the longitudinal and lateral directions, respectively; b, $w1$, and $w2$ indicate the carbody, leading axle, and trailing axle of the vehicle, respectively, and M and I represent the mass and mass-inertia of the wheelset or carbody, respectively.

The damping and stiffness matrices of the vehicle are also square matrices of 7 order, which can be expressed as $[C_V] = c_1[S_V]$ and $[K_V] = k_1[S_V]$ respectively, where $[S_V]$ is the matrix of geometrical coefficients presented below:

$$[S_v]_{7\times7} = \begin{bmatrix} 2 & 0 & 0 & 0 & -2 & 0 & d_w \\ 0 & \frac{1}{2}d_p^2 & 0 & 0 & 0 & -\frac{1}{2}d_p^2 & 0 \\ 0 & 0 & 2 & 0 & -2 & 0 & -d_w \\ 0 & 0 & 0 & \frac{1}{2}d_p^2 & 0 & -\frac{1}{2}d_p^2 & 0 \\ -2 & 0 & -2 & 0 & 4 & 0 & 0 \\ 0 & -\frac{1}{2}d_p^2 & 0 & -\frac{1}{2}d_p^2 & 0 & d_p^2 & 0 \\ d_w & 0 & -d_w & 0 & 0 & 0 & d_w^2 \end{bmatrix}, \quad (2)$$

and c_1 and k_1 are the damping and stiffness of the primary suspension of the vehicle, respectively.

The track superstructure system comprises the rails, the sleepers, and the concrete slab. The Euler-Bernoulli beam theory used for modelling the rail elements (e.g. main and auxiliary rails). The rail elements are meshed with 200 mm length. The sleepers are also simulated with Euler-Bernoulli beams. By neglecting the torsional rotation, each node of beam elements considered with five DOFs including of three translations and two rotations. The rail fastening system is simulated as spring-damper elements. These spring-damper elements are used to connect the rails to the slab (or sleepers).

The concrete slab track and approach slab were modelled by an ensemble of longitudinal and transversal grids of Euler-Bernoulli beams. Fig. 6 shows the mesh discretization adopted for the grid of beams representing the reinforced concrete slab. The distance of grid beams in longitudinal direction is 150 mm and the transversal beams were meshed in adapting of sleeper elements. The schematic section view of sleeper (or slab) mesh is shown in Fig. 7. The transversal beams of slab and sleeper have same meshed just that the slab beams have one more element with 200 mm length at the end edges. The first two elements of the sleeper beam have coarser mesh (150 mm) and the others has finer mesh (125 mm). The consideration of the stiffer concrete components with a grid of beams instead of solid elements was adopted in order to not only assure an adequate representation of the bending behavior of these elements, but also avoid extremely low time-steps in the integration procedure, which would be required with equivalent solid elements. This choice allowed a computation time reduction of a factor of about 2.5 in this study.

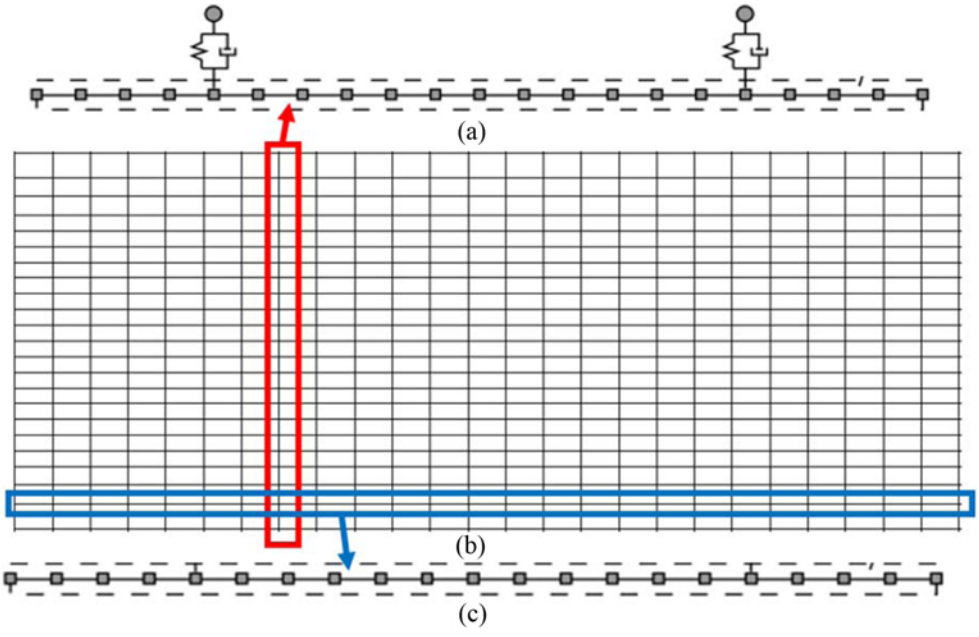

Fig. 6. Slab Track Model: (a) Longitudinal Beam Elements, (b) Grid of Beam Elements, (c) Transversal Beam Elements

The substructure system comprises the lean concrete layer, the FPL, the prepared subgrade, sub-ballast, all the other soil layers underneath, and the approach slab. Except for the approach slab, all the components were modeled with low-order fully integrated eight-node solid hexahedral elements. The approach slab was modeled with a grid of Euler-Bernoulli beams. The mesh size of the sublayers of sleeper and slab elements are matched with the sleeper or slab meshes as shown in Fig. 7. The ballast-substructure system of the model composed of brick elements with hexahedral meshes as depicted in Fig. 8. A good representation of the dynamic motion is obtained with a minimum of ten (loworder) elements per wavelength (Kuhlemeyer and Lysmer, 1973; Wood, 2004). The maximum size of the finite elements is therefore given by lmax = λ/10, where λ is the wavelength. The wavelength relates to the waves velocities and to the corresponding frequencies, according to $\lambda = v/f$. The maximum size of the finite elements is thus found with the minimum wave velocity of the materials (the shear wave velocity) and the maximum frequency of interest.

The absorption of waves in the boundaries of the model were made with local dashpots with properties tuned to minimize reflections (Lysmer and Kuhlemeyer, 1969). For this goal, a series of viscoelastic dashpots were used to absorb the propagating waves on lateral boundaries of the model.

3.2 Vehicle-Track-Substructure Interaction

As the program divides the railway system into three main subsystems, the total model can be generated by assembling the equations of the motion of vehicle, track superstructure, and substructure with regard to their interaction contacts. Thus, the total equations of the motion of the model can be established by:

$$[M]\{a\}+[C][v]+[K]\{u\} = \{F\}\,, \tag{3}$$

where $\{a\}$, $\{v\}$, $\{u\}$, and $\{F\}$ are the vectors of nodal displacements, velocities, accelerations, and external forces of the complete system, respectively, and $[M]$, $[C]$, and $[K]$ are the total mass, damping, and stiffness matrices of the model, respectively, which can be derived by assembling the related submatrices as:

$$\begin{bmatrix} M_V & 0 & 0 \\ 0 & M_T & 0 \\ 0 & 0 & M_S \end{bmatrix}\begin{bmatrix} a_V \\ a_T \\ a_S \end{bmatrix}+\begin{bmatrix} C_V & 0 & 0 \\ 0 & C_T & 0 \\ 0 & 0 & C_S \end{bmatrix}\begin{bmatrix} v_V \\ v_T \\ v_S \end{bmatrix}+\begin{bmatrix} K_V & 0 & 0 \\ 0 & K_T & 0 \\ 0 & 0 & 0 \end{bmatrix}\begin{bmatrix} u_V \\ u_T \\ u_S \end{bmatrix}=\begin{bmatrix} F_{gV}+F_{V/T} \\ F_{gT}-F_{V/T}+F_{T/S} \\ F_{gS}-F_{T/S} \end{bmatrix}. \tag{4}$$

The subscripts V, T, and S are used to address the vehicle subsystem, the track superstructure subsystem, and the substructure subsystem, respectively, the load vectors F_{gV}, F_{gT} and F_{gS} denote the corresponding gravity forces, as well as $F_{V/T}$ and $F_{T/S}$are the vectors of the vehicle-track and track-substructure interaction forces.

The time-domain solution for these equilibrium equations was obtained by means of a mixed explicit-implicit integration technique (detailed in Varandas et al., 2017) where the vehicle and the substructure subsystem equations were integrated with Zhai's explicit scheme (Zhai, 1996), and the track superstructure subsystem was integrated with Newmark's implicit scheme.

The contacts between the three main subsystems of the model are the vehicle-track and track-substructure interactions. For computing the vehicle-track interaction forces, the Hertz contact theory was considered (Lankarani and Nikravesh, 1990; Vale and Calçada, 2014). Therefore, the vector of the vehicle-track interaction force, which corresponds to a wheel-rail contact, can be derived by the following equation:

where k_H is the normal stiffness coefficient and $(u_{V;i}-u_{T;i})$ is the relative displacement between the ith wheel and the rail on the

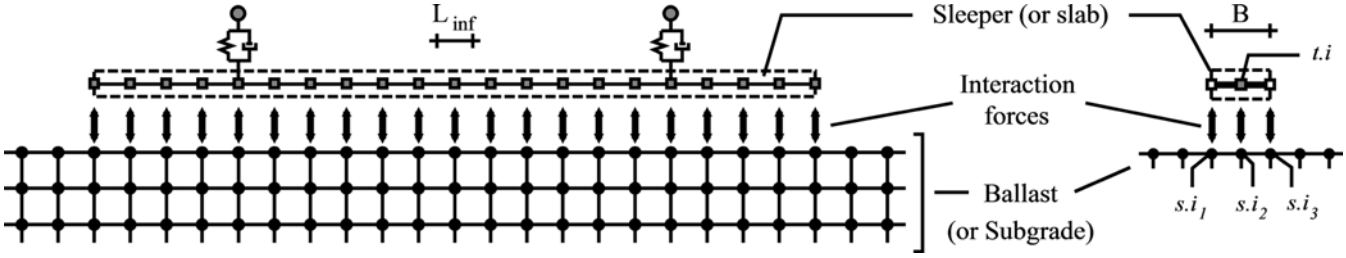

Fig. 7. Interactions Model of Track-Substructure

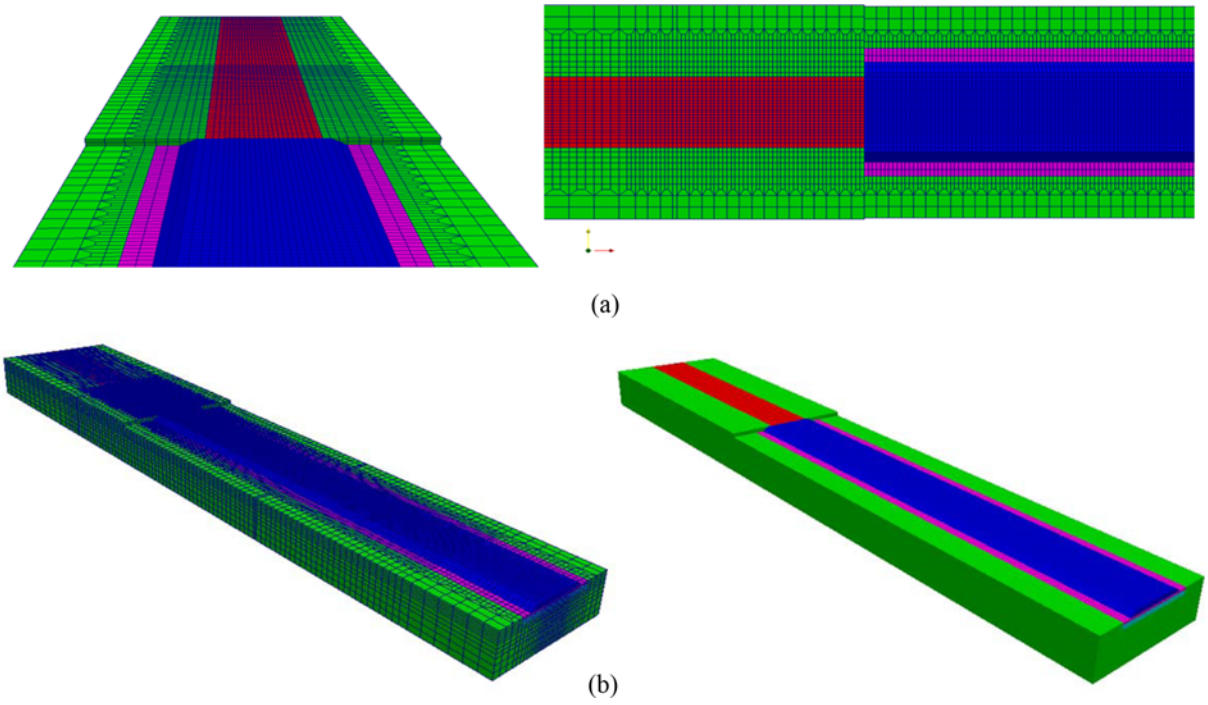

Fig. 8. Slab-Ballasted Track Model: (a) Plan and Top View, (b) 3D View with and without Mesh

contact position.

$$F_{V/T;i} = \begin{cases} k_H(u_{V;i} - u_{T;i})^{1.5} & ; \textit{in contact} \\ 0 & ; \textit{otherwise}, \end{cases} \quad (5)$$

The contact between the track and substructure can be defined at the superposed nodes of sleeper (or slab) and the ballast (or lean concrete) layer as shown in Fig. 7. The vector of the superstructure-substructure interaction forces is calculated using the following equations:

$$F_{T/S;j} = \begin{cases} c_{c;j}(v_{T;j} - v_{S;j}) + k_{c;j}(u_{T;j} - u_{S;j}) & ; \textit{in contact} \\ 0 & ; \textit{otherwise}, \end{cases} \quad (6)$$

where j indicates the superposed nodes of sleeper (or slab) and substructure elements, $F_{T/S,j}$ is their vertical interaction force, $k_{c.j}$ and $c_{c.j}$ are the corresponding stiffness and damping, $v_{T;j}$ and $v_{S;i}$ represent the vertical velocities, and $U_{T;j}$ and $u_{S;i}$ denote the vertical displacements of the jth nodes of the sleeper (or slab) and substructure.

3.3 Model Characteristics

A 3D view of the numerical model representing the studied slab-ballasted track transition is shown in Fig. 8. The characteristics of the track components are listed in Table 1. In addition, the total width and length of the model are 9.1 and 52.20 m, respectively. The transition zone, made with two parts, has a total length of 18 m, as shown in Fig. 1. The total number of rail-supports, elements, and degrees-of-freedom are 88, 137350, and 450216, respectively.

3.4 Model Validation

As described in section 2, the displacements of the rail in four positions in the case-study segment were recorded during the passage of a test vehicle. This track vehicle has two wheel-axles with a distance of 6.50 m weighting 13 and 10 tons, respectively.

The results obtained from the modeling and the experimental measurements along the railway track (for slab and ballasted tracks as well as transition parts 1 and 2) are compared in Fig. 9. As can be observed in this figure, the trends of the measurement and the numerical results are nearly similar and the values of displacements have a good agreement with each other. It is also

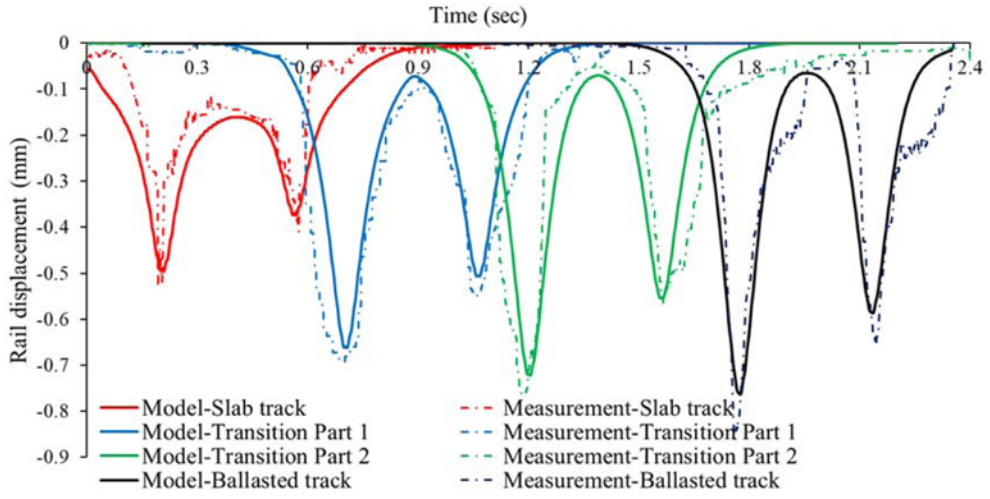

Fig. 9. Comparison of Model and Measurement Results at the Slab Track, Combined Transition Zone and Ballasted Track

seen that the track stiffness decreases from the slab track to the ballasted track and that the transition segment promotes a smooth transition between these two parts.

4. Results and Discussion

In this section, the performance of the studied transition zone is investigated using several parametric analyses. To this aim, several parameters of the vehicle and track were modified in multiple dynamic analyses, and this section presents the results obtained for the analyses of the parameters that most significantly affected the dynamic response of the track transition.

4.1 Influence of Vehicle Parameters

The train speed and axle load values are the two main factors that most significantly influence the dynamic response of the railway track. Therefore, in this section, the effect of the train speed is evaluated by changing the speed values in the range of 120 km/h to 300 km/h, and the influence of the axle load is surveyed for typical values of 180, 220, and 250 kN.

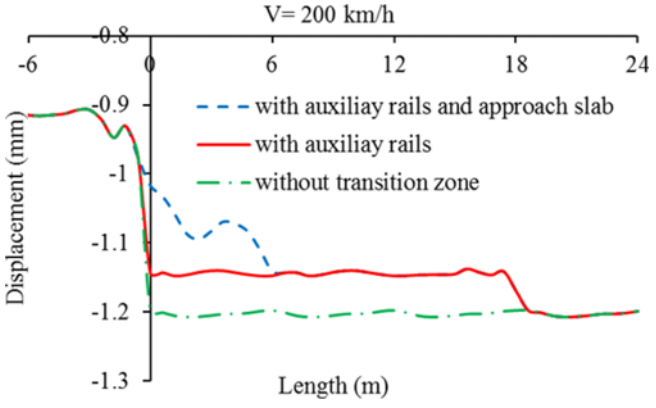

Fig. 10. Comparison of the Rail Displacement Variations for Different Transition Zones (auxiliary rails, approach slab and their combined system)

Figure 10 shows the comparison of rail displacement variations along different transition zones (auxiliary rails, approach slab and their combined system) for vehicle speed of 200 km/h and axle load of 180 kN. As depicted in this figure, the combined

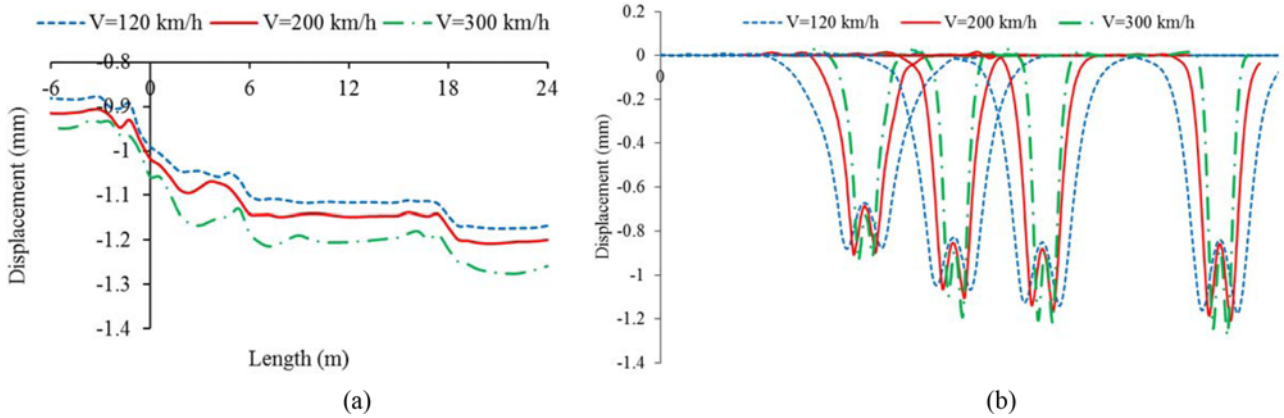

Fig. 11. Rail Displacements for Various Train Speeds along the Combined Transition Zone: (a) Maximum Downward Rail Displacements, (b) Rail Displacement Profiles at Four Locations (Identified in Fig. 3)

transition system creates milder variation as three steps gradually.

Figure 11 shows the variation of the maximum downward rail displacements along the studied track segment when the vehicle with 180 kN axle load travels from the slab track to the ballasted track for different values of train speeds (120, 200 and 300 km/h). As shown in this figure, it can be found that the rail displacements along the transition zone with auxiliary rails and an approach slab generally occur in three steps, therefore promoting a gradual stiffness transition, in contrast to the solution with auxiliary rails only (two steps) or the solution without a transition zone (single abrupt step). These diagrams also demonstrate that the downward displacements generally tend to increase with the train speed and that the response for speeds in the range of 200 – 300 km/h presents significant dynamic components, whereas the response obtained at 120 km/h is not far from a quasi-static regime. It is also observed that for the higher train speeds, the ballast on top of the approach slab vibrates vertically due to the strong reduction of radiation damping as a result of the introduction of the stiff approach slab underneath.

Another vehicle parameter that significantly affects the dynamic performance of railway transition zones is the axle load value. Therefore, the values of the axle load were changed within a common range for typical railway vehicles (180, 220, and 250 kN) and the influence of the applying loads on the combined transition zone was studied. The track displacement variation along the transition zone for a fixed speed of 200 km/h is

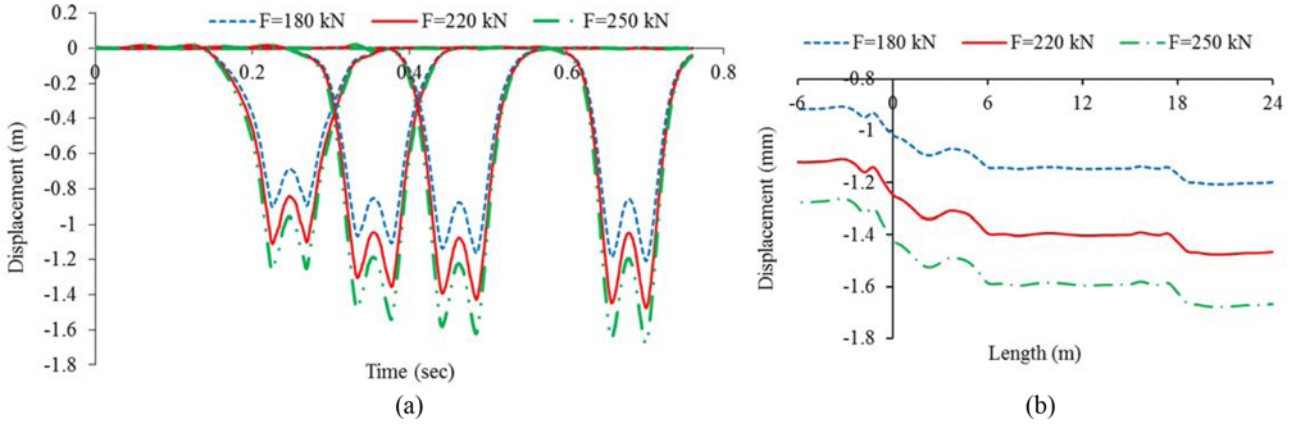

Fig. 12. Rail Displacements for Various Axle Loads along the Combined Transition Zone: (a) Rail Displacement Profiles at Four Locations (Identified in Fig. 3), (b) Maximum Downward Rail Displacements

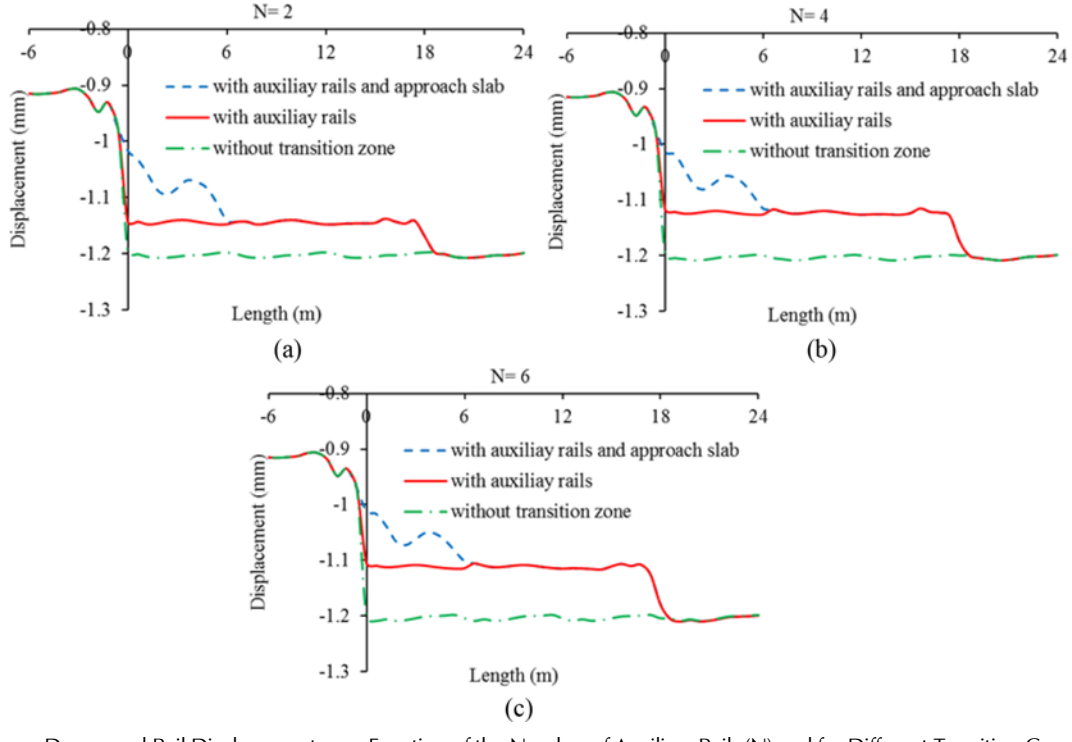

Fig. 13. Maximum Downward Rail Displacements as a Function of the Number of Auxiliary Rails (N) and for Different Transition Cases: (a) N = 2, (b) N = 4, (c) N = 6

depicted in Fig. 12. As shown in this figure, the increase of axle load values leads to elevated deformation of the track, but the general profile variation remains unchanged. In particular, the average rail displacements from the initial slab track section to the final ballasted track section increase about 34% for all axle load values, while this amplification is reduced to 22% and 28% at the first and second parts of the combined transition zone, irrespective of the axle load value.

4.2 Influence of Track Parameters

Among the various track parameters that can be selected to investigate the influence of the combined transition zone, sensitive analyses were performed on the most influencing parameters of the track response such as the stiffness of the fastening system (Thölken et al., 2021) and changing the number of auxiliary rails. These parameters had a significant impact on the performance of the combined transition zone, as will be shown in the following section.

Figure 13 shows the maximum downward rail displacements that were obtained with a variable number of auxiliary rails (N) ranging from N = 2 to N = 6, considering a fixed speed of 200 km/h. As can be seen, the addition of two auxiliary rails has a clear effect on reducing the rail displacement variation, but the introduction of the supplementary two or four rails (N = 4 or N = 6) has a smaller relative advantage. These results suggest that additional auxiliary rails should be generally implemented with N = 2. However, the consideration of N = 4 might be acceptable in cases with very abrupt stiffness transition, ideally with a progressive transition in terms of auxiliary rails number: from N = 4 to N = 2 to N = 0.

Sensitive analyses on the railpad stiffness value were performed by changing the vertical stiffness by three values of 40, 110, and 250 kN/mm, which are the soft, medium, and hard elasticity conditions, respectively. These analyses were carried out by passing a vehicle with 180 kN axle loads and 200 km/h velocity. Figs. 14 and 15 show the comparison of the transition zone displacements (with auxiliary rails, approach slab, and their combination system) for the mentioned vertical stiffness values of the fastening system. These figures indicate that the medium to hard stiffness condition shows minor differences, but the soft stiffness railpad leads to a very significant increase in terms of track displacements. On the other hand, when the displacement difference between the consecutive track segments forming the transition is examined, it is observed that the soft railpad provides a less stiff transition between the segments: Considering average downward displacement values within segments, depending on the railpad stiffness value (40, 110, or 250 kN/mm), the displacements increase from the slab track segment to the final ballasted track segment by 18%, 35%, and 38%, respectively. Moreover, for the segment with auxiliary rails only, the displacements increase from the slab track segment is 15%, 28%, and 30%, respectively. This shows that the soft railpad stiffness value promotes a natural smoothness of the track transition stiffness profile, which can be further increased by adopting railpads with varied stiffness values between transition segments.

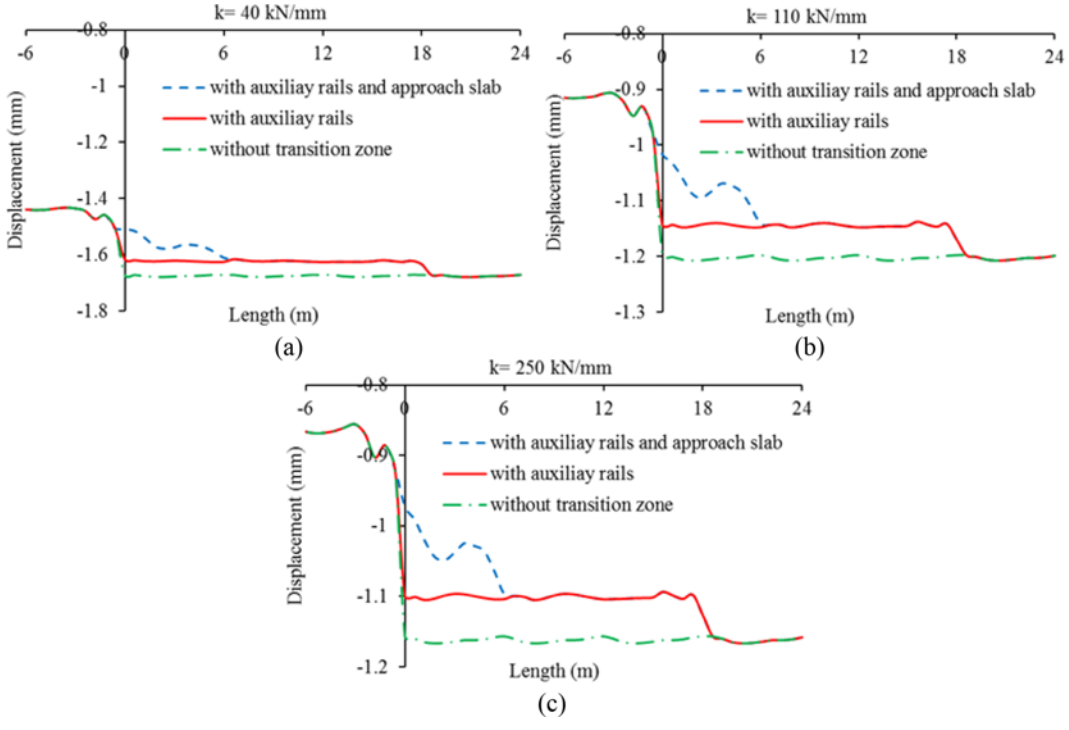

Fig. 14. Maximum Downward Rail Displacements as a Function of the Vertical Stiffness of the Fastening System (K), and for Different Transition Cases: (a) K = 40 kN/mm, (b) K = 110 kN/mm, (c) K = 250 kN/mm

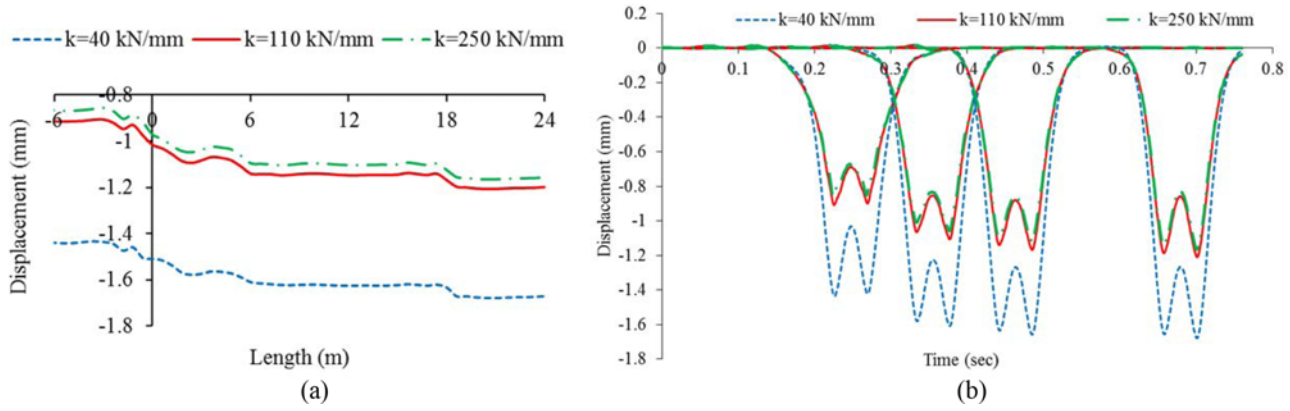

Fig. 15. Rail Displacements for Various Vertical Stiffnesses of the Fastening System (40, 110 and 250 kN/mm) along the Combined Transition Zone: (a) Maximum Downward Rail Displacements, (b) Rail Displacement Profiles at Four Locations (identified in Fig. 3)

5. Conclusions

1. In this paper, the effect of a combined system for the slab-ballasted track transition is investigated by numerical modeling. For this purpose, a 3D railway track model, which was based on the FE method and contained three segments including the slab track segment, the transition zone, and the ballasted track segment, was initially validated using the measured track displacements during the passage of a track maintenance vehicle. The validated model was then used to study the impact of several vehicle and track parameters on the behavior of the combined transition zone. The main obtained results are listed below: The combined system, considering a transition zone formed by auxiliary rails and an approach slab, promotes a smoother stiffness transition between the slab track segment and the ballasted track segment, by making this transition in three gradual steps.
2. An increasing train speed promotes generally higher displacements, and higher speed values further increase the appearance of dynamic effects, mostly seen on top of the approach slab. In low and medium speeds (e.g. 120 and 200 km/h), the track variations are approximately occurred same together in three steps (22.5%, 28% and 34.5%). But in high speeds (e.g. 300 km/h), the variations of the track displacements in each of steps are occurred in higher ranges with regard to the low and medium speeds (29%, 34% and 41%).
3. By using of the combined transition zone for all axle applying loads, the rail displacements are respectively increased about 22%, 28% and 34% at the first transition part, second transition section and ballasted track with comparing of slab track values.
4. An increasing number of auxiliary rails can be beneficial in terms of reducing the stiffness transition, but it is noted that the greatest advantage is attained with only two auxiliary rails. Therefore, a higher number of auxiliary rails may be adopted only in cases of very high train speeds and possibly with a gradual variation in numbers.
5. The numerical results also suggest that lower stiffness railpads can be beneficial in smoothing the track stiffness transition, irrespective of the adopted transition system: no transition, transition with auxiliary railways only, or combined transition with auxiliary rails and an approach slab.

Altogether, the obtained results corroborate that the studied combined transition system promotes a beneficial step-by-step stiffness transition, and therefore, is an adequate measure in junction points of the slab track and the ballasted track. Additional studies are planned to analyze the influence of high train speeds on the ballast behavior located above the approach slab, on the appropriate length of the approach slab as a function of the maximum train speed, and on the possibility of complementary systems, such as the adoption of railpads with variable stiffness values along the transition.

Acknowledgments

Not Applicable

ORCID

Hamidreza Heydari-Noghabi https://orcid.org/0000-0003-3768-2415
José Nuno Varandas https://orcid.org/0000-0002-7083-1278
Jabbar Ali Zakeri https://orcid.org/0000-0002-4946-7192
Morteza Esmaeili https://orcid.org/0000-0002-8189-5584

References

Aggestam E, Nielsen J (2019) Multi-objective optimisation of transition zones between slab track and ballasted track using a genetic algorithm. *Journal of Sound and Vibration* 446:91-112, DOI: 10.1016/j.jsv.2019.01.027

Arlaud E, Costa D'Aguiar S, Balmès E, Faussurier G (2016) Numerical study of railway track dynamics: Case of a transition zone. Proceedings of the third international conference on railway technology: Research, development and maintenance, Cagliari, Italy 1-20

Bhatti MA (2005) Fundamental finite element analysis and applications: With mathematica and matlab computations. John Wiley & Sons Inc, 1st edition, New Jersey, United States

Coelho BZ, Hicks MA (2015) Numerical analysis of railway transition zones in soft soil. *Proceedings of the Institution of Mechanical Engineers, Part F: Journal of Rail and Rapid Transit* 230(6):1601-1613, DOI: 10.1177/0954409715605864

Costa D'Aguiar S, Arlaud E, Potvin R, Laurans E, Funfschillling C (2015) Railway transitional zones: A case history from ballasted to ballastless track. *International Journal of Railway Technology* 3(1): 37-61, DOI: 10.4203/ijrt.3.1.2

Esmaeili M, Heydari-Noghabi H, Kamali M (2020) Numerical investigation of railway transition zones stiffened with auxiliary rails. *Proceedings of the Institution of Civil Engineers: Transport* 173(5):299-308, DOI: 10.1680/jtran.17.00035

Fei J, Xiao J, Jie Y, Han K, Yang C (2019) In-situ test study on compaction control parameters for particular subdivisional railway earthworks. *International Journal of Pavement Engineering* 22(10):1295-1304, DOI: 10.1080/10298436.2019.1683177

Haoyu W (2018) Measurement, assessment, analysis and improvement of transition zones in railway track. PhD Thesis, Delft University of Technology, DOI: 10.4233/uuid:73830b2c-deb1-4da9-b19c-5e848c5cfa4d

Heydari H, Zakeri JA, Esmaeili M (2022) Evaluating the elastic sleeper efficiency in reduction of railway ground vibrations by in situ impact-response test. *International Journal of Vehicle Noise and Vibration* 17(3-4):237-252, DOI: 10.1504/IJVNV.2022.10046110

Heydari-Noghabi H, Varandas JN, Esmaeili M, Zakeri J (2017) Investigating the influence of auxiliary rails on dynamic behavior of railway transition zone by a 3D train-track interaction model. *Latin American Journal of Solids and Structure* 14(11):2000-2018, DOI: 10.1590/1679-78253906

Heydari-Noghabi H, Zakeri JA, Esmaeili M, Varandas JN (2018) Field study using additional rails and an approach slab as a transition zone from slab track to the ballasted track. *Proceedings of the Institution of Mechanical Engineers, Part F: Journal of Rail and Rapid Transit* 232(4):970-978, DOI: 10.1177/0954409717708527

Hughes TJR (2003) The finite element method. Dover Publications Inc, New York, United States

Kuhlemeyer RL, Lysmer J (1973) Finite element method accuracy for wave propagation problems. *Journal of the Soil Mechanics and Foundations Division*, 99(5):421-427

Lankarani HM, Nikravesh PE (1990) A contact force model with hysteresis damping for impact analysis of multibody systems. *ASME Journal of Mechanical Design* 112:369-376, DOI: 10.1115/1.2912617

Lei X, Zhang B (2010) Influence of track stiffness distribution on vehicle and track interactions in track transition. *Proceedings of the Institution of Mechanical Engineers, Part F: Journal of Rail and Rapid Transit* 224(6):592-604, DOI: 10.1243/09544097JRRT318

Lysmer J, Kuhlemeyer RL (1969) Finite dynamic model for infinite media. *Journal of the Engineering Mechanics Division* 95(4):859-77, DOI: 10.1061/JMCEA3.0001144

MATLAB (2010) version 7.10.0 (R2010a). Natick, Massachusetts: The MathWorks Inc.

Miller K, Joldes G, Lance D, Wittek A (2007) Total Lagrangian explicit dynamics finite element algorithm for computing soft tissue deformation. *Communications in Numerical Methods in Engineering* 23(2):121-134, DOI: 10.1002/cnm.887

Ngamkhanong C, Ming QY, Li T, Kaewunruen S (2020) Dynamic train-track interactions over railway track stiffness transition zones using baseplate fastening systems. *Engineering Failure Analysis* 118:104866, DOI: 10.1016/j.engfailanal.2020.104866

Paixão A, Fortunato E, Calcada R (2013) Design and construction of backfills for railway track transition zones. *Proceeding of Institution of Mechanical Engineers, Part F: Journal of Rail and Rapid Transit* 229(1): 58-70, DOI: 10.1177/0954409713499016

Paixão A, Fortunato E, Calcada R (2013) Design and construction of backfills for railway track transition zones. *Proceeding of Institution of Mechanical Engineers, Part F: Journal of Rail and Rapid Transit* 229(1):58-70, DOI: 10.1177/0954409713499016

Paixão A, Ribeiro CA, Pinto N, Fortunato E, Calçada R (2015) On the use of under sleeper pads in transition zones at railway underpasses: Experimental field testing. *Structure and Infrastructure Engineering* 11(2):112-128, DOI: 10.1080/15732479.2013.850730

Real T, Zamorano C, Hernández, García JA, Real JI (2016) Static and dynamic behavior of transitions between different railway track typologies. *KSCE Journal of Civil Engineering* 20(4):1356-1364, DOI: 10.1007/s12205-015-0635-2

Sañudo R, Dell'Olio L, CasadoJosé JA, Diego S (2016) Track transitions in railways: A review. *Construction and Building Materials* 112:140-157, DOI: 10.1016/j.conbuildmat.2016.02.084

Sasaoka D, Davies D (2005) Implementing track transition solutions for heavy axle load service. AREMA 2005, Corpus ID: 197675494

Shahraki M, Warnakulasooriya C, Witt KJ (2015) Numerical study of transition zone between ballasted and ballastless railway track. *Transportation Geotechnics* 3:58-67, DOI: 10.1016/j.trgeo.2015.05.001

Thölken D, Abdalla Filho JE, Pombo J, Sainz-Aja J, Carrascal I, Polanco J, Esen A, Laghrouche O, Woodward P (2021) Three-dimensional modelling of slab-track systems based on dynamic experimental tests. *Transportation Geotechnics* 31:100663, DOI: 10.1016/j.trgeo.2021.100663

Vale C, Calçada R (2014) A dynamic vehicle-track interaction model for predicting the track degradation process. *Journal of Infrastructure Systems* 20(3):04014016-1-13, DOI: 10.1061/(ASCE)IS.1943-555X.0000190

Varandas JN (2013) Long-term behaviour of railways transitions under dynamic loading: Application to soft soil sites. Universidade NOVA de Lisboa, Dept. of Civil Engineering, PhD Thesis, http://hdl.handle.net/10362/10145

Varandas JN, Paixão A, Fortunato E (2017) A study on the dynamic train-track interaction over cut-fill transitions on buried culverts. *Computers and Structures* 189:49-61, DOI: 10.1016/j.compstruc.2017.04.017

Varandas JN, Paixão A, Fortunato E, Zuada Coelho B, Hölscher P (2020) Long-term deformation of railway tracks considering train-track interaction and non-linear resilient behaviour of aggregates – a 3D FEM implementation. *Computers and Geotechnics* 126:103712, DOI: 10.1016/j.compgeo.2020.103712

Walker R, Indraratna B (2018) Moving loads on a viscoelastic foundation with special reference to railway transition zones. *International Journal of Geomechanics* 18(11), DOI: 10.1061/(ASCE)GM.1943-5622.0001274

Wang H, Markine VL (2018a) Methodology for the comprehensive analysis of railway transition zones. *Computers and Geotechnics* 99:64-79, DOI: 10.1016/j.compgeo.2018.03.001

Wang H, Markine VL (2018b) Modelling of the long-term behaviour of transition zones: Prediction of track settlement. *Engineering Structures* 156: 294-304, DOI: 10.1016/j.engstruct.2017.11.038

Wang H, Markine VL, Liu X (2017) Experimental analysis of railway track settlement in transition zones. *Proceedings of the Institution of Mechanical Engineers, Part F: Journal of Rail and Rapid Transit* 232(6):1774-1789, DOI: 10.1177/0954409717748789

Wang H, Markine VL, Shevtsov IY, Dollevoet R (2015) Analysis of the dynamic behaviour of a railway track in transition zones with

differential settlement. *Proceedings of the 2015 Joint Rail Conference*, American Society of Mechanical Engineers, San Jose, California, USA. March 23-26, DOI: 10.1115/JRC2015-5735

Wood DM (2004) Geotechnical modelling. CRC Press, 1st edition, London. ISBN 0-415-34304-6, DOI: 10.1201/9781315273556

Xin T, Ding Y, Wang P, Gao L (2020) Application of rubber mats in transition zone between two different slab tracks in high-speed railway. *Construction and Building Materials* 243:118219, DOI: 10.1016/j.conbuildmat.2020.118219

Zakeri JA, Ghorbani V (2011) Investigation on dynamic behavior of railway track in transition zone. *Journal of Mechanical Science and Technology* 25:287-292, DOI: 10.1007/s12206-010-1202-x

Zhai WM (1996) Two simple fast integration methods for Large-Scale dynamic problems in engineering. *International Journal for Numerical Methods in Engineering* 39(24):4199-4214, DOI: 10.1002/(SICI)1097-0207(19961230)39:24<4199::AID-NME39>3.0.CO;2-Y